ChemComm

COMMUNICATION

View Article Online
View Journal | View Issue

Cite this: *Chem. Commun.*, 2024, **60**, 7319

Received 9th February 2024,
Accepted 7th May 2024

DOI: 10.1039/d4cc00683f

rsc.li/chemcomm

Cyano disubstituted tetrabenzoindeno[2,1-*a*]fluorene: open-shell or closed-shell?†

Priyank Kumar Sharma,[a] Palash Jana,[b] Subhajit Bandyopadhyay[b] and Soumyajit Das *[a]

Organic diradicaloids have lately emerged as potential spintronic materials. We report the unprecedented synthesis of a near-IR absorbing indeno[2,1-*a*]fluorene derivative that displays remarkably low LUMO (−4.15 eV) and a small HOMO–LUMO gap (0.85 eV). NMR/EPR studies indicated its open-shell diradical property, which was supported by DFT calculations while suggesting a 30% diradical character and a small singlet (S)–triplet (T) gap (−2.52 kcal mol^{-1}). A large bond length alternation of the *as*-indacene core for its single-crystals indicated a quinoidal contribution with greater antiaromaticity, which is in line with the small diradical character despite showing a small S–T gap.

Exploration of polycyclic hydrocarbons (PHs) with antiaromatic and diradical properties has attracted immense interest in recent years,[1] as tuning such properties may provide paths toward new organic semiconductor materials with tunable band gaps. Formally antiaromatic indeno[1,2-*b*]fluorene[2] **1** and indeno[2,1-*a*]fluorene[3] **2** regioisomers are stable closed-shell (CS) molecules that display moderate antiaromaticity for the central *s*-indacene and *as*-indacene units,[4] respectively (Fig. 1a). Unsymmetrical disubstitution of [2,1-*a*]IF also resulted in a stable CS molecule **3**,[5] but benzo-extension of the central *as*-indacene unit of [2,1-*a*]IF afforded an open-shell (OS) molecule **benzo-2** with a large diradical character index (y_0 = 0.63), likely causing instability (half-life 77 min) and 8% synthetic yield.[6]

In continuation of efforts[7] to synthesize the elusive arene-fused dicyclopenta[*b*,*d*]thiophene (DCPT),[7a,b] a diphenanthro-DCPT (**DPDCPT**) derivative was targeted (Fig. 1b). While attempting its synthesis by a DDQ (2,3-dichloro-5,6-dicyano-1,4-benzoquinone) mediated dehydrogenation from dihydro precursor **2H-DPDCPT**, we failed to isolate it presumably due to the high reactivity (electron-rich, large y_0 = 0.51, and a small singlet–triplet energy gap (ΔE_{S-T}) = −0.64 kcal mol^{-1}; Table S2, ESI†), as analysed by density functional theory (DFT) calculation. Instead, we isolated a cyano disubstituted tetrabenzoindeno[2,1-*a*]fluorene **6** (Fig. 1b) as a degradation product, and it was confirmed by single-crystal X-ray diffraction (SCXRD) analysis (*vide infra*). Isolation of **6** was interesting since there is no straightforward synthetic approach known thus far to construct **5**, which is a constitutional isomer of known tetrabenzoindeno[1,2-*b*]fluorene **4**,[8] which displays a greater degree of antiaromaticity for the *s*-indacene unit than that of **1**. Our DFT optimization of **5** indicated its CS ground state, like **4**, and its OS singlet state was found to be isoenergetic with the CS state with a small ΔE_{S-T} = −3.46 kcal mol^{-1} (Table S2, ESI†). A lowering of the triplet state for **5**, despite showing a negligible diradical character (y_0 = 0.01), is in line with a recent report[9] by

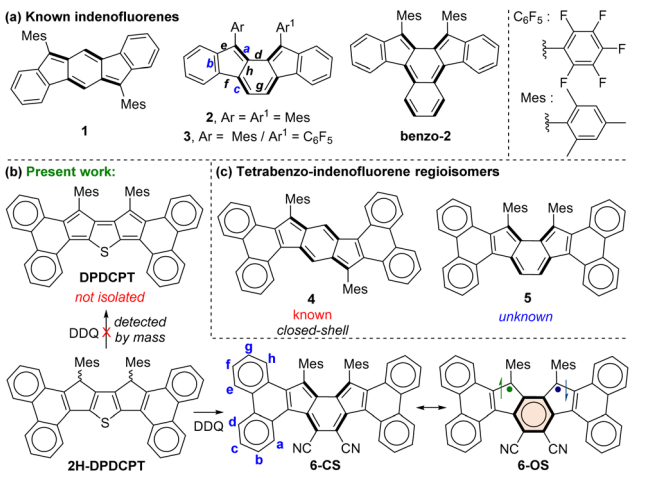

Fig. 1 (a) Indeno[1,2-*b*]fluorene **1**, indeno[2,1-*a*]fluorenes **2** & **3**, and benzo-fused [2,1-*a*]IF **benzo-2**. (b) Targeted diphenanthro-DCPT, and the synthesized tetrabenzoindeno[2,1-*a*]fluorene **6** and its resonance forms. (c) Isomeric tetrabenzoindeno[1,2-*b*]fluorene **4** and tetrabenzoindeno[2,1-*a*]fluorene **5** derivatives.

[a] *Department of Chemistry, Indian Institute of Technology Ropar, Rupnagar 140001, Punjab, India. E-mail: chmsdas@iitrpr.ac.in*
[b] *Department of Chemical Sciences, Indian Institute of Science Education and Research (IISER) Kolkata, Mohanpur 741246, West Bengal, India*

† Electronic supplementary information (ESI) available: Detailed syntheses and characterization data for **6**; X-ray crystallographic data; DFT calculations; NMR spectra; direct mass spectrum of **DPDCPT**; and plausible mechanism for formation of **6**. CCDC 2309430. For ESI and crystallographic data in CIF or other electronic format see DOI: https://doi.org/10.1039/d4cc00683f

Ottosson and Solà *et al.* explaining that diphenanthro-fused antiaromatics (pentalene, *s*-indacene) may display low-lying triplet states. Despite the lowering of the triplet excited state, **5** didn't show an OS ground state, theoretically.

We envisaged that the cyano (–CN) substituents for **6** may result in a smaller HOMO–LUMO energy spacing than that of **5**, seemingly due to the greater stabilization effect exerted by electron-withdrawing –CN groups (negative resonance effect), which are attached to *as*-indacene carbons containing large LUMO coefficients (Fig. S22, ESI†).[10] A small HOMO–LUMO energy gap is crucial to show an OS ground state, as evident from CS heptazethrene-triisopropylsilylethynyl (**HZ-TIPS**)[11] *vs.* OS heptazethrene-dicarboximide (**HZ-DI**),[12] though the number of Clar sextet recoveries remains the same for them. Therefore, in this work, compound **6** was thoroughly studied by various analytical techniques and DFT calculations to conclude its electronic ground state, while reporting its unprecedented synthesis.

Suzuki coupling between commercially available **7** and 2,5-dibromothiophene-3,4-dicarbaldehyde **8**,[13] as depicted in Scheme 1, afforded dialdehyde derivative **9**. Treatment of **9** with 2-mesitylmagnesiumbromide afforded a diol intermediate, which was subsequently treated with $BF_3{\cdot}Et_2O$ to give **2H-DPDCPT**, which is the dihydro precursor of **DPDCPT**. DDQ-mediated oxidative dehydrogenation of **2H-DPDCPT** in dichloromethane (DCM) remained partially complete, even after refluxing or increasing the reaction time, as monitored by thin layer chromatography. To ensure complete conversion, 4 equiv. DDQ was added, and the reactant was consumed within 30 minutes at room temperature (rt). The formation of the targeted **DPDCPT** could be detected from the crude reaction mixture by direct mass spectrometric (MS) analysis (Fig. S25, ESI†), but unfortunately, no desired product trace was obtained after traditional silica gel column chromatography; instead, **DPDCPT-DDQ** was isolated as a 10+2 cycloaddition adduct,[14] likely due to the reaction of **DPDCPT** and DDQ on the silica surface (Fig. S26, ESI†).

Treatment of silica gel with triethylamine, prior to loading the slurry of the crude reaction mixture containing DDQ, afforded a deep purple solid in 42% yield. However, the high-resolution mass (m/z = 739.3099) didn't match the desired mass of **DPDCPT**. It was found to be an unexpected product **6** after SCXRD analysis of the purple solid (Fig. 2), plausibly formed by

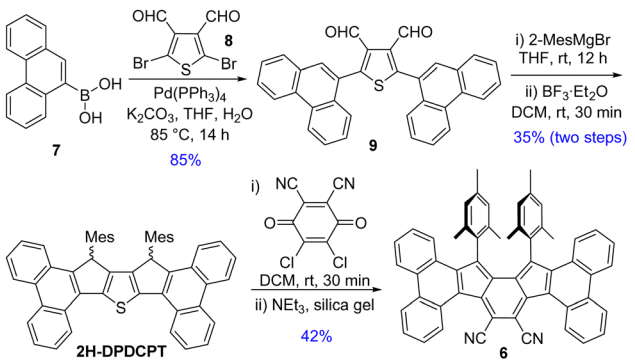

Scheme 1 Synthesis of **6**.

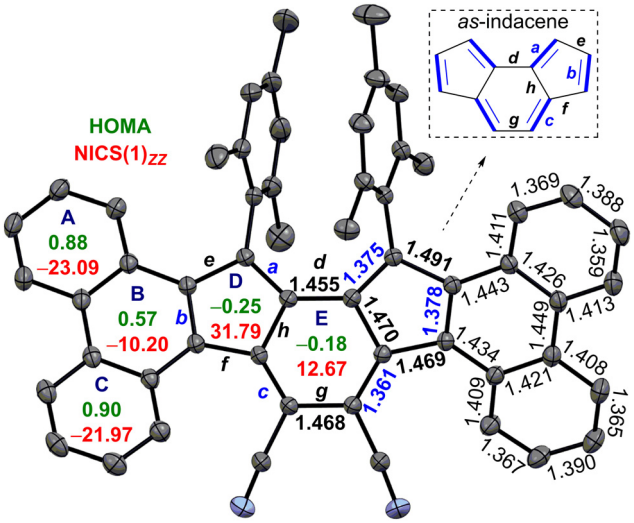

Fig. 2 ORTEP drawing of **6** with thermal ellipsoids at the 30% probability level (hydrogens and disordered solvent omitted), including the mean bond lengths (in angstroms), NICS(1)$_{zz}$ (red) and HOMA (green) indices.

the loss of a sulfur atom and ClC(═C═O)C(Cl)═C═O unit from the **DPDCPT-DDQ** adduct on neutral silica gel or an alumina column (Fig. S26, ESI†).[14b,c] Nonetheless, **6** is the first diphenanthro-*as*-indacene derivative with an *ortho*-quinoidal backbone, which is a structural isomer of **4**.

The single crystals of **6** were grown in a DCM/acetonitrile mixture (Fig. 2). SCXRD analysis of **6** revealed a contorted π-backbone (Fig. S13a, ESI†) due to the steric congestion between the –CN group and ring-C hydrogen in the cove region and repulsive interaction between the bulky mesityl groups, which are orthogonal to the IF backbone. The terminal phenanthrene units were twisted by an avg. torsional angle of 30.1°, as measured from the mean planes between central ring E and outer phenanthrene units (Fig. S13a, ESI†). The C–C double bond *b* linking *as*-indacene and the phenanthrene unit and the *exo*-methylene bond *a* for **6** are 0.032 Å and 0.016 Å, respectively, shorter than those of **2** (Fig. 2 and Table 1). The C–C single bonds *d*–*h* for **6** possess more single bond character (1.455 to 1.491 Å), with *e* and *g* bonds 0.016 and 0.037 Å longer than those of **2**. The degree of bond length alternation (BLA) in the *as*-indacene unit has significantly enhanced for **6** in comparison to **2**, suggesting a reduced extent of π-delocalization for the *as*-indacene core in **6**, indicating a greater degree of antiaromaticity for **6** than that of **2**. On the other hand, the homogeneous bond length distribution for rings A (avg. 1.394 Å) and C (avg. 1.393 Å) in **6** suggested a greater degree of benzene-like aromaticity than that of ring B (avg. 1.425 Å).

The harmonic oscillator model of aromaticity (HOMA)[15] analyses of the optimized structure **6** (at BHandHLYP/6-31G*)

Table 1 Mean C_{sp^2}–C_{sp^2} crystal bond lengths (*a*–*h*, in Å) of **6** *vs.* **2**, for *as*-indacene

	a	*b*	*c*	*d*	*e*	*f*	*g*	*h*
6	1.375	1.378	1.361	1.455	1.491	1.469	1.468	1.470
2	1.391	1.410	1.359	1.454	1.475	1.463	1.431	1.480

supported the large BLA for rings D (−0.25) and E (−0.18), whereas small (A = 0.88, C = 0.90) to moderate (B = 0.57) BLA for phenanthrene indicated its aromaticity (Fig. 2). Nuclear independent chemical shift (NICS)[16] calculation showed larger positive NICS(1)$_{zz}$ values for rings D (31.79) and E (12.67) for **6** than those of **2**, suggesting enhanced antiaromaticity of the *as*-indacene unit for **6**. The negative NICS values of rings A (−23.09), B (−10.20), and C (−21.97) for **6** are in line with the HOMA values, supporting phenanthrene ring aromaticity.

The observation of proton NMR (nuclear magnetic resonance) line broadening for **6** at rt (Fig. S5, ESI†) prompted us to study its variable temperature (VT) NMR behaviour. In $CDCl_3$, **6** exhibited broad NMR signals for some of the aromatic protons (d, c, b protons in Fig. 3a, see Fig. 1b for proton labels) at rt, while other ring protons were also broadened upon heating (Fig. S9, ESI†). These broad NMR signals became sharper upon gradual cooling and became reasonably sharper at −60 °C (213 K). This is a typical observation for OS diradicaloid PHs with small ΔE_{S-T},[11,17] due to which the excited triplet state can be thermally populated at rt or by slight heating. The observation was also supported by VT-EPR (electron paramagnetic resonance), exhibiting a featureless broad signal (g_e = 2.0041) at rt, while the signal intensity decreased as the temperature was lowered from 260 K to 150 K (Fig. 3b), which is a consequence of reduced population of magnetically active triplet species at lower temperatures.[18] A careful fitting of the VT-EPR data using the Bleaney–Bowers equation[19] gave a ΔE_{S-T} = −0.97 kcal mol^{-1} for **6** (Fig. S11a, ESI†), suggesting singlet OS ground state, which is in line with VT-EPR in solution (ΔE_{S-T} = −1.73 kcal mol^{-1}, Fig. S11b and c, ESI†).

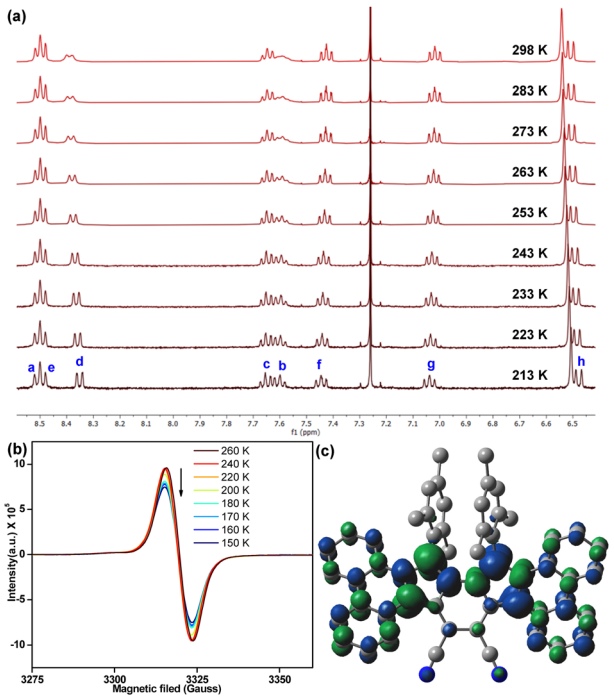

Fig. 3 (a) Partial VT-NMR of **6** in $CDCl_3$ showing aromatic protons (see Fig. 1b for proton labels); (b) VT-EPR spectra of solid sample **6**; (c) spin density distribution of singlet OS **6**.

DFT calculation of **6** at the BHandHLYP/6-31G* level of theory[20] confirmed that the energy of an OS singlet state was 1.96 kcal mol^{-1} and 2.52 kcal mol^{-1} lower than the energy of the CS singlet (quinoidal) and triplet (biradical) states, respectively (Table S2, ESI†). The y_0 for **6** was estimated to be 0.30, based on the natural orbital occupation numbers using the broken symmetry formalism. The frontier molecular orbital profiles for α- and β-spins (Fig. S21, ESI†) displayed the characteristic disjointed nature in the ground state singlet diradical form. The spin densities were observed to be uniformly dispersed across the entire π-conjugated framework (Fig. 3c), giving thermodynamic stability.

The UV-vis-NIR (UV-visible-near infrared) spectrum (Fig. 4a) of **6** exhibited intense absorption peaks at λ_{max} = 312 nm (ε = 30 000 M^{-1} cm^{-1}) and λ_{max} = 365 nm (ε = 19 000 M^{-1} cm^{-1}) in the UV region and a moderate absorption in the visible region λ_{max} = 554 nm (ε = 11 000 M^{-1} cm^{-1}), which is associated with a weak absorption band in the lowest energy region stretching from 750 to 1500 nm in the NIR region with the absorption maximum at λ_{max} = 1000 nm (ε = 650 M^{-1} cm^{-1}). Time dependent-DFT (TD-DFT) calculations of **6** in toluene (Fig. S19, ESI†) suggested that the absorption in the visible region is dominated by the HOMO−1 → LUMO transition (λ_{max} = 476 nm, oscillator strength (f) = 0.55, Table S3, ESI†), while the weaker lowest energy absorption tail has originated from a forbidden HOMO → LUMO transition (λ_{max} = 877 nm, f = 0.028). Such a long wavelength absorption tail could originate due to the admixing of the doubly excited electronic configuration (H,H → L,L) for **6** owing to its OS ground state, as observed for Kubo's diphenaleno-DCPT.[14a] Compound **6** displayed a very small optical HOMO–LUMO energy gap of 0.85 eV, as roughly estimated from the lowest energy absorption onset (1240/λ_{onset}); yet, a good photostability under ambient conditions with a half-life of 9 days was observed for **6** (Fig. S10, ESI†).

Cyclic voltammetry (CV) and differential pulse voltammetry (DPV) analyses (Fig. 4b) suggested that **6** could be easily reversibly reduced at $E_{1/2}^{red1}$ = −0.73 V and at $E_{1/2}^{red2}$ = −1.16 V (*vs.* ferrocene/ferrocenium (Fc/Fc$^+$) couple). It can also be oxidized to its radical cation and dication species at E_{peak}^{ox1} = 0.68 V and E_{peak}^{ox2} = 0.93 V, respectively. The HOMO and LUMO energy levels were −5.40 eV and −4.15 eV, as estimated from the onset potentials of the oxidation and reduction waves, respectively, giving a small electrochemical energy gap of 1.25 eV. The LUMO energy level of **6** is remarkably stabilized (low-lying) due to the electron-withdrawing cyano substituents, as hypothesized.

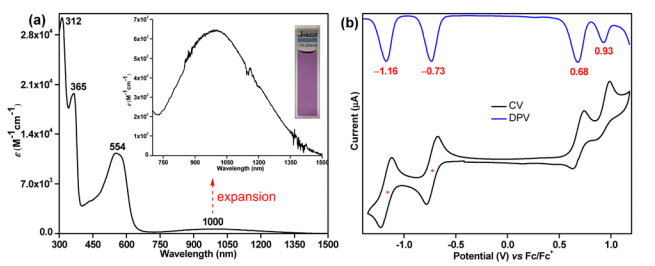

Fig. 4 (a) UV-vis-NIR absorption spectrum of **6** in toluene (715–1500 nm expansion shown in inset); (b) CV and DPV of **6**.

The greater stabilization of the LUMO basically reduced the HOMO–LUMO energy gap, and the observation is comparable to **HZ-TIPS** *vs.* **HZ-DI**, where **HZ-DI** with a small HOMO–LUMO gap displayed an OS diradicaloid ground state despite one Clar sextet being recovered for both molecules in their OS forms.[11,12] The smaller ΔE_{S-T} for **6** than that of **5** could be caused by the narrower HOMO–LUMO gap of **6** pushing its triplet excited state to locate closer to the singlet ground state.[21] As a result, the excited triplet state could be easily thermally populated at rt or by slight heating, despite showing a small y_0. Usually, the greater the y_0, the smaller the ΔE_{S-T};[22] with a few noteworthy exceptions[23] (including **benzo-2**)[6] showing a larger ΔE_{S-T} although exhibiting a larger y_0. To the best of our knowledge, compound **6** is a unique example that exhibits a small y_0 despite showing a small ΔE_{S-T}.

Typically, an OS PH with large y_0 displays a large energy difference between its CS singlet and OS singlet states, and a small energy difference between its OS singlet state and first excited triplet state.[24] Our experimental and theoretical studies confirmed that **6** exists as an OS diradicaloid in the singlet ground state with its CS quinoidal state lying in between the OS ground state and triplet excited state, which is unlike the known diradicaloid PHs[17,24] with large y_0 displaying CS quinoidal states lying vertically at a much higher energy level above the triplet state. A significant BLA for the central *as*-indacene unit of **6** in its crystalline form indicates a dominant quinoidal structure presumably due to the rt accessible low-lying CS state, which is in line with the small y_0. This observation suggested that both CS and OS resonance forms for **6** may contribute to the singlet ground state.

In summary, a formally antiaromatic diphenanthro-*as*-indacene derivative **6** was synthesized, that exhibits diradical-like and antiaromatic properties in its OS singlet ground state as a result of a low-lying CS state. Though the formation of **6** was unexpected, its detailed characterization gave newer insights in diradical chemistry as our study suggested that substitution driven HOMO–LUMO energy gap modulation can affect the ground state properties for antiaromatic PHs. The small y_0 (30%) for **6** could likely be attributed to the dominant *as*-indacene antiaromaticity owing to the low-lying quinoidal CS form, as supported by SCXRD analysis and NICS(1)$_{zz}$ calculation. The VT-NMR and VT-EPR experiments indicated its singlet diradicaloid ground state, which is the consequence of a small HOMO–LUMO energy gap. Qualitative correlations between the structural features and the properties of different diradicaloid systems usually indicate an increased y_0 as the energy separation between the singlet and triplet states decreased. However, compound **6** is an example of a rare diradicaloid exhibiting a small y_0 despite showing a small ΔE_{S-T}, implying potential for applications in organic spintronics and photonics (non-linear optics and singlet-fission) studies.[25]

S. D. thanks SERB, India (CRG/2022/003012) for funding. P. K. S. and P. J. thank CSIR for the senior research fellowship. S. B. thanks SERB for a research grant (CRG/2022/006776). The authors thank Kamlesh Satpute (IIT Ropar) for SCXRD data of **6**.

Conflicts of interest

There are no conflicts to declare.

Notes and references

1 (*a*) A. Konishi, Y. Okada, M. Nakano, K. Sugisaki, K. Sato, T. Takui and M. Yasuda, *J. Am. Chem. Soc.*, 2017, **139**, 15284; (*b*) T. Xu, X. Hou, Y. Han, H. Wei, Z. Li and C. Chi, *Angew. Chem., Int. Ed.*, 2023, **62**, e202304937.
2 D. T. Chase, A. G. Fix, S. J. Kang, B. D. Rose, C. D. Weber, Y. Zhong, L. N. Zakharov, M. C. Lonergan, C. Nuckolls and M. M. Haley, *J. Am. Chem. Soc.*, 2012, **134**, 10349.
3 A. Shimizu and Y. Tobe, *Angew. Chem., Int. Ed.*, 2011, **50**, 6906.
4 Y. Tobe, *Top. Curr. Chem.*, 2018, **376**, 12.
5 H. Sharma, N. Bhardwaj and S. Das, *Org. Biomol. Chem.*, 2022, **20**, 8071.
6 H. Miyoshi, S. Nobusue, A. Shimizu, I. Hisaki, M. Miyata and Y. Tobe, *Chem. Sci.*, 2014, **5**, 163.
7 (*a*) X. Shi and C. Chi, *Top. Curr. Chem.*, 2017, **375**, 68; (*b*) P. K. Sharma, D. Mallick and S. Das, *Org. Lett.*, 2023, **25**, 5089; (*c*) X. Shi, P. Mayorga Burrezo, S. Lee, W. Zhang, B. Zheng, G. Dai, J. Chang, J. T. López Navarrete, K.-W. Huang, D. Kim, J. Casado and C. Chi, *Chem. Sci.*, 2014, **5**, 4490; (*d*) G. E. Rudebusch, A. G. Fix, H. A. Henthorn, C. L. Vonnegut, L. N. Zakharov and M. M. Haley, *Chem. Sci.*, 2014, **5**, 3627.
8 C. K. Frederickson, L. N. Zakharov and M. M. Haley, *J. Am. Chem. Soc.*, 2016, **138**, 16827.
9 R. Ayub, O. El Bakouri, K. Jorner, M. Solà and H. Ottosson, *J. Org. Chem.*, 2017, **82**, 6327.
10 A. Casey, S. D. Dimitrov, P. Shakya-Tuladhar, Z. Fei, M. Nguyen, Y. Han, T. D. Anthopoulos, J. R. Durrant and M. Heeney, *Chem. Mater.*, 2016, **28**, 5110.
11 Y. Li, W.-K. Heng, B. S. Lee, N. Aratani, J. L. Zafra, N. Bao, R. Lee, Y. M. Sung, Z. Sun, K.-W. Huang, R. D. Webster, J. T. López Navarrete, D. Kim, A. Osuka, J. Casado, J. Ding and J. Wu, *J. Am. Chem. Soc.*, 2012, **134**, 14913.
12 Z. Sun, K.-W. Huang and J. Wu, *J. Am. Chem. Soc.*, 2011, **133**, 11896.
13 P. K. Sharma, D. Mallick, H. Sharma and S. Das, *Org. Lett.*, 2023, **25**, 2201.
14 (*a*) T. Kubo, M. Sakamoto, M. Akabane, Y. Fujiwara, K. Yamamoto, M. Akita, K. Inoue, T. Takui and K. Nakasuji, *Angew. Chem., Int. Ed.*, 2004, **43**, 6474; (*b*) Z.-L. Wang, H.-L. Li, L.-S. Ge, X.-L. An, Z.-G. Zhang, X. Luo, J. S. Fossey and W.-P. Deng, *J. Org. Chem.*, 2014, **79**, 1156; (*c*) J. S. Li, Y. Xue, Z. W. Li, W. D. Liu, C. H. Lu and P. X. Zhao, *Synlett*, 2013, **24**, 2003.
15 T. Lu and F. Chen, *J. Comput. Chem.*, 2012, **33**, 580.
16 H. Fallah-Bagher-Shaidaei, C. S. Wannere, C. Corminboeuf, R. Puchta and P. V. R. Schleyer, *Org. Lett.*, 2006, **8**, 863.
17 (*a*) S. Das, S. Lee, M. Son, X. Zhu, W. Zhang, B. Zheng, P. Hu, Z. Zeng, Z. Sun, W. Zeng, R.-W. Li, K.-W. Huang, J. Ding, D. Kim and J. Wu, *Chem. – Eur. J.*, 2014, **20**, 11410; (*b*) P. Yadav, S. Das, H. Phan, T. S. Herng, J. Ding and J. Wu, *Org. Lett.*, 2016, **18**, 2886.
18 P. Jana, S. Koppayithodi, S. Mahato, S. Molla and S. Bandyopadhyay, *J. Phys. Chem. Lett.*, 2023, **14**, 7433.
19 B. Bleaney and K. D. Bowers, *Proc. R. Soc. London, Ser. A*, 1952, **214**, 451.
20 S. Lehtola, M. Dimitrova, H. Fliegl and D. Sundholm, *J. Chem. Theory Comput.*, 2021, **17**, 1457.
21 W. Zeng, Q. Qi and J. Wu, *Eur. J. Org. Chem.*, 2018, **2018**, 7.
22 J. J. Dressler and M. M. Haley, *J. Phys. Org. Chem.*, 2020, **33**, e4114.
23 (*a*) J. J. Dressler, M. Teraoka, G. L. Espejo, R. Kishi, S. Takamuku, C. J. Gómez-García, L. N. Zakharov, M. Nakano, J. Casado and M. M. Haley, *Nat. Chem.*, 2018, **10**, 1134; (*b*) J. E. Barker, J. J. Dressler, A. Cárdenas Valdivia, R. Kishi, E. T. Strand, L. N. Zakharov, S. N. MacMillan, C. J. Gómez-García, M. Nakano, J. Casado and M. M. Haley, *J. Am. Chem. Soc.*, 2020, **142**, 1548.
24 S. S. K. Boominathan, K.-H. Chang, Y.-C. Liu, C.-S. Wang, C.-F. Wu, M.-H. Chiang, P.-T. Chou and Y.-T. Wu, *Chem. – Eur. J.*, 2019, **25**, 7280.
25 (*a*) S. Datta, Y. Cai, I. Yudhistira, Z. Zeng, Y.-W. Zhang, H. Zhang, S. Adam, J. Wu and K. P. Loh, *Nat. Commun.*, 2017, **8**, 677; (*b*) M. Nakano, *Chem. Rec.*, 2017, **17**, 27.

